The Pennsylvnia State University
APPLIED RESEARCH LABORATORY
Post Office Box 30
State College, PA 16804

Fluid Film Bearing Dynamic Coefficients and Their Application to Structural Finite Element Models

by

R. L. Campbell

Technical Report 03-007
August 1, 2003

E. G. Liszka, Director
Applied Research Laboratory

REPORT DOCUMENTATION PAGE

Form Approved OMB No. 0704-0188

1. REPORT DATE *(DD-MM-YYYY)*	2. REPORT TYPE	3. DATES COVERED *(From - To)*
01-08-2003	Technical Report	

4. TITLE AND SUBTITLE
Fluid Film Bearing Dynamic Components and Their Application to Structural Finite Element Models

5a. CONTRACT NUMBER

5b. GRANT NUMBER

5c. PROGRAM ELEMENT NUMBER

6. AUTHOR(S)
R. L. Campbell

5d. PROJECT NUMBER

5e. TASK NUMBER

5f. WORK UNIT NUMBER

7. PERFORMING ORGANIZATION NAME(S) AND ADDRESS(ES)

Applied Research Laboratory
Post Office Box 30
State College, PA 16804

8. PERFORMING ORGANIZATION REPORT NUMBER

TR 03-007

9. SPONSORING / MONITORING AGENCY NAME(S) AND ADDRESS(ES)
Applied Research Laboratory
Post Office Box 30
State College, PA 16803

10. SPONSOR/MONITOR'S ACRONYM(S)
ARL/PSU

11. SPONSOR/MONITOR'S REPORT NUMBER(S)

12. DISTRIBUTION / AVAILABILITY STATEMENT

Approved for public release, distribution unlimited

13. SUPPLEMENTARY NOTES

14. ABSTRACT

A review of methods currently employed for modeling static and dynamic characteristics of fluid film bearings is provided. In nearly all cases, the literature discusses the use of dynamic coefficients for low-order rotor-dynamics models in which a single stiffness and damping matrix is used to connect an individual rotor node to an individual stator/bearing node along the shaft centerline. The focus of the present work is on developing dynamic coefficients for high-order structural finite element models, which use a distribution of the coefficients over the journal circumference. While the methods presented here are applicable to many bearing types, the focus is on the most common bearing, the plain and tilting pad bearing designs. A numerical study is provided to show the importance of properly implementing the bearing coefficients by comparing the results for two methods of coefficient implementation for a rotor model. The results show differences in rotor-to-stator transfer accelerance, resonance frequencies, and damping levels.

15. SUBJECT TERMS

16. SECURITY CLASSIFICATION OF:			17. LIMITATION OF ABSTRACT	18. NUMBER OF PAGES	19a. NAME OF RESPONSIBLE PERSON
a. REPORT	b. ABSTRACT	c. THIS PAGE	UU		19b. TELEPHONE NUMBER *(include area code)*
UNCLASSIFIED	UNCLASSIFIED	UNCLASSIFIED	UNCLASSIFIED-UNLIMITED	30	

TABLE OF CONTENTS

LIST OF TABLES

LIST OF FIGURES

LIST OF SYMBOLS

C = bearing radial clearance
C' = pivot point circle clearance
F = force
G = turbulent correction factor
H = characteristic height
I = pad rotational inertia
L = bearing width
M = pad equivalent mass
N = number of pads
R = journal radius
R_p = pad radius
Re = Reynolds number = ratio of viscous to inertial forces
Re^* = modified Reynolds number
T = coordinate transformation matrix
V = Velocity
W = applied load
b = damping component
e = journal eccentricity
h = film thickness
k = stiffness component
m = preload
p = pressure
t = time
x = global coordinate in direction of applied load W
y = global coordinate in direction perpendicular to x and in bearing plane
Ω = angular speed of journal relative to bearing
α = angle between pad start and pivot location (measured in $+\theta$-direction)
ε = journal eccentricity ratio = e/C
ϕ = attitude angle
η = local coordinate in direction perpendicular to ξ
γ = pad angle
μ = lubricant kinematic viscosity
ρ = lubricant density
θ = angular coordinate
ξ = local coordinate passing through pad center of curvature and pad pivot point
ω = pad vibration frequency
ψ = pad location (measured from negative x-direction)

1 Introduction

Rotor systems are often constructed using either rolling element or journal bearings to enable relative angular motion between the rotor shaft and the system housing. Rotor dynamics and structural finite element models of such systems generally use linear elastic elements (linearized about a normal operating point) to represent the coupling characteristics of these components instead of employing complicated bearing models that must be solved simultaneously with the system model. The process of determining the coupling characteristics of both types of bearings can be complicated, but for different reasons. The difficulty for rolling element bearings is mainly a result of having a discrete number of rolling elements (see Figure 1.1a), which causes the stiffness to be highly nonlinear since the number of rolling elements in contact with the raceway at any given time depends on the amount of shaft deflection. A detailed discussion of rolling element bearing modeling is out of the scope of this report. Instead, the reader is referred to the discussion of this topic provided in Reference 1.

Unlike rolling element bearings, journal bearings are difficult to model because their stiffness and damping depends on a hydrodynamic lubrication layer with characteristics that are largely controlled by the relative velocity of the bearing and journal surfaces, lubrication viscosity, and bearing geometry. This layer exists in the fluid region between the shaft and the journal as shown in Figure 1.1b. The ability of the fluid film to carry a load is a result of a converging fluid film gap caused by eccentricity of the journal relative to the bearing and the presence of a viscous fluid. The result of these conditions is a viscous shear flow that yields a net hydrodynamic force in the gap that can support a load with no direct journal-to-bearing contact (and hence no bearing wear).

There are a variety of hydrodynamic journal bearing designs used for rotating equipment [2], most of which are a variation of the common plain bearing design. Some of the usual variations include the multi-lobed and tilting pad designs shown in Figure 1.2. Often, the intent of the design modifications is to enhance the overall stability of the rotor system. From a modeling perspective, the modifications result in a more complex system. For low order (1-dimensional) shaft/housing models, methods are available to derive net stiffness and damping characteristics at the shaft centerline. Higher order models that attempt to simulate the dynamic behavior around

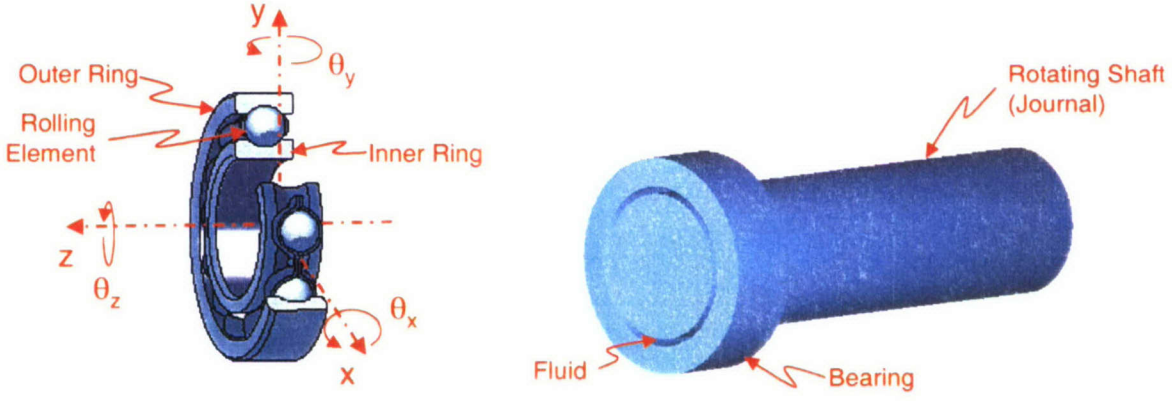

Figure 1.1. (a) Rolling element bearing schematic, and (b) plain journal bearing schematic.

the housing and shaft circumference require distributed stiffness and damping representations of the bearings. For example, a rim-drive motor finite element model may require the application of circumferentially varying forces or the prediction of response harmonics in the circumferential direction and thus a distribution of the bearing coefficients around the journal circumference is required. It is the intent of this report to summarize the methods currently used to approximate the equivalent dynamic characteristics for the plain journal bearing and the tilting pad bearing and introduce a method to circumferentially distribute these coefficients for use in a structural finite element model. As previously stated, the plain journal bearing and the tilting pad bearing are being focused on here because they are two of the most commonly employed bearings for rotating equipment.

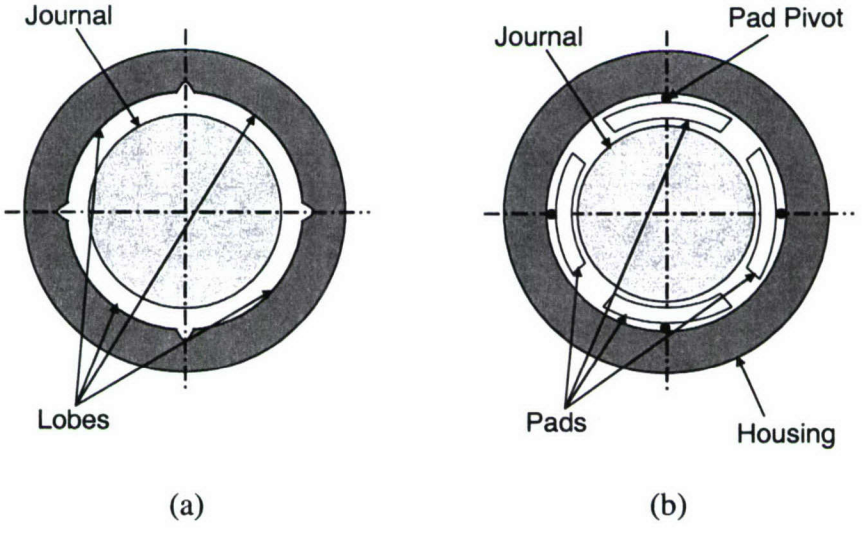

Figure 1.2. (a) Four-lobed bearing, and (b) tilting pad bearing.

2 Background

The process of computing bearing dynamic coefficients begins with solving for the pressure field in the fluid film between the journal and bearing surfaces. The equation used for this purpose is referred to as the *Reynolds equation*. Important aspects of this partial differential equation are highlighted next, along with boundary conditions and methods to solve the system.

2.1 The Reynolds Equation

The film pressure in a journal bearing is generally computed using the *Reynolds equation* shown below[1] [4,5,6,7].

[1] An informative historical review of hydrodynamic lubrication theory and the development of the Reynolds equation can be found in Reference 3.

$$\frac{1}{R}\frac{\partial}{\partial\theta}\left(\frac{h^3}{12\mu}\frac{1}{R}\frac{\partial p}{\partial\theta}\right)+\frac{\partial}{\partial z}\left(\frac{h^3}{12\mu}\frac{\partial p}{\partial z}\right)=\frac{1}{2}\Omega\frac{\partial h}{\partial\theta}+\frac{\partial h}{\partial t}, \tag{2.1}$$

where h is the film thickness, μ is the lubricant viscosity, p is the fluid film pressure, R is the bearing radius, t is time, Ω is the angular speed of the journal relative to the bearing, z is the coordinate along the axis of rotation, and θ represents rotation about z. The derivation of Equation 2.1 begins with the Navier-Stokes and continuity equations and employs several assumptions, including the following:[2]

- effects of bearing curvature are negligible (i.e., centrifugal forces are neglected),
- pressure variation across the fluid film is negligible,
- the flow is laminar,
- fluid inertia effects are negligible when compared to the viscous effects,[3]
- the flow is incompressible, and
- the fluid viscosity is constant.

For turbulent flow, turbulent correction factors, G_θ and G_z, obtained from Hirs bulk-flow theory [9,10] are often added to Reynolds equation to approximately account for the turbulence effects. Using these factors, the Reynolds equation becomes:

$$\frac{1}{R}\frac{\partial}{\partial\theta}\left(G_\theta\frac{h^3}{\mu}\frac{1}{R}\frac{\partial p}{\partial\theta}\right)+\frac{\partial}{\partial z}\left(G_z\frac{h^3}{\mu}\frac{\partial p}{\partial z}\right)=\frac{1}{2}\Omega\frac{\partial h}{\partial\theta}+\frac{\partial h}{\partial t}, \tag{2.2}$$

where

$$G_\theta=\frac{2^{1+m}}{n(2+m)}\mathrm{Re}^{-(1+m)}, \text{ and} \tag{2.3}$$

$$G_z=\frac{2^{1+m}}{n}\mathrm{Re}^{-(1+m)}. \tag{2.4}$$

For flows with smooth surfaces and Reynolds numbers ($\mathrm{Re}=\frac{\rho Vh}{\mu}$) less than 10^5, common values for n and m are: $n = 0.066$ and $m = -0.25$ [11]. For laminar flow, G_θ and G_z are both equal to $\frac{1}{12}$.

---

[2] Inherent to the Navier-Stokes equations is the assumption of a Newtonian fluid. For non-Newtonian fluids, a lubrication rheological model may be necessary (see Reference 8 for an introduction to lubrication rheology).

[3] The consequence of this assumption is that all terms in the Navier-Stokes equations that are multiplied by $\varepsilon\mathrm{Re}$ are neglected when $\varepsilon\mathrm{Re} << 1$ ($\varepsilon = H/L$, $\mathrm{Re} = \rho V\cdot H/\mu$, H is a characteristic film thickness, L is the bearing width, V is a characteristic velocity, and μ is a characteristic fluid viscosity).

Note that the derivation of the Reynolds equation assumes negligible fluid inertia effects. This assumption is supported when the modified Reynolds number, $\mathrm{Re}^* = \frac{\rho V C}{\mu} \frac{C}{R}$, is much less than unity. For cases when this criterion is not met, methods presented in References 10 and 16 should be used to account for the inertia effects.[4] Also note that the Reynolds equation assumes constant fluid viscosity within the fluid film. Methods to incorporate a variable viscosity due to thermal effects are presented in References 17, 18, and 19.

2.2 Boundary Conditions

The choice of appropriate boundary conditions for the Reynolds equation has been the topic of much discussion over the years, focusing mainly on how the film rupture boundary condition is handled. In fact, boundary conditions that are compatible to both the boundary pressure and continuity are yet to be defined [16]. Film rupture may occur at the 'downstream' boundary if a diverging film exists at this location. For a plain journal bearing, a diverging film will always occur at the downstream boundary ($\theta_2 = \pi+\phi$ in Figure 2.1). However, short-length pads often have a converging film over the entire surface (see Figure 2.2 for a schematic of a bearing with short length pads).

There are two types of boundary conditions that are commonly used: the Reynolds conditions

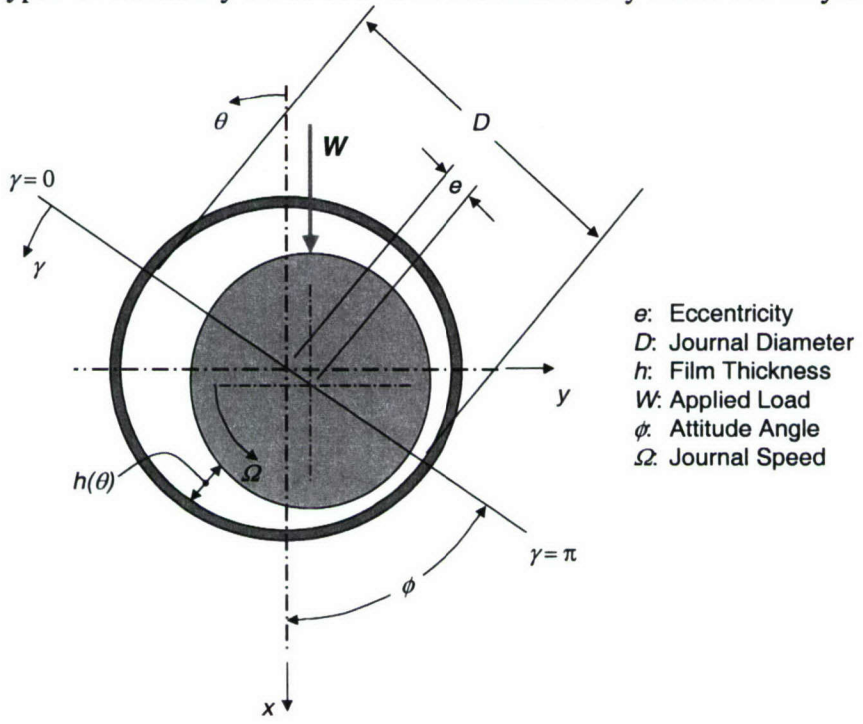

Figure 2.1. Plain journal bearing variables.

[4] Reference 10 reports that as *C/R* decreases, the results from the equations that include inertia effects decrease monotonically to the results of the classical theory. Thus, it may be acceptable to neglect inertia effects when *C/R* is small.

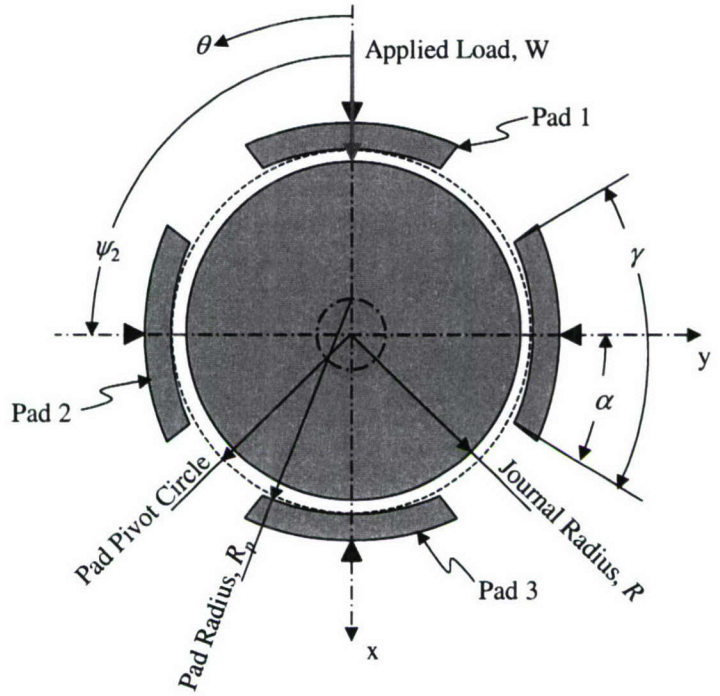

Figure 2.2. Tilting pad journal bearing analysis variables.

($p(\theta_2)=\left.\frac{\partial p}{\partial \theta}\right|_{\theta_2}=0$) and Gumbel's conditions. The Reynolds conditions are applied by setting every term of negative pressure to zero during the solution process, and Gumbel's conditions suggest that all pressures in the solution that are less than atmospheric pressure be ignored[5] [16]. While neither method maintains flow continuity, the theoretical results obtained from using either of these conditions have been shown to closely match experimental data [16].

2.3 Reynolds Equation Solution

Closed solutions to the Reynolds equation (Equation 2.1) have been developed for two simplified conditions [4]: an infinitely long bearing (*Sommerfeld* or *long bearing* solution), and an infinitely short bearing (*Ocvirk* or *short bearing* solution), both of which are summarized in the Appendix. The Sommerfeld solution is applicable to bearings with length (L) to diameter (D) ratios large enough that leakage from the bearing ends is small relative to the flow in the circumferential direction (i.e., $L/D >> 1$), whereas the Ocvirk solution is applicable to bearings with $L/D < \sim 1$ such that end leakage is significant. Because most bearings in use have L/D ratios in the range of ¼ to 1, the Ocvirk solution is often applicable [4].

In order to avoid the limiting assumptions of these simplified solutions, the Reynolds equation is often solved numerically using finite difference [12,13], finite element [11], or other methods wherein the solution is obtained from a search for the minimum value of the functional [11]:

[5] This is sometimes called the *half-Sommerfeld* approach.

$$J(p)=\int_{-\frac{L}{2}}^{\frac{L}{2}}\int_{\theta_1}^{\theta_2}\left\{\frac{G_\theta h^3}{2R^2\mu}\left(\frac{\partial p}{\partial\theta}\right)^2+\frac{G_z h^3}{2\mu}\left(\frac{\partial p}{\partial z}\right)^2+\left(\frac{\Omega}{2}\frac{\partial h}{\partial\theta}+\frac{\partial h}{\partial t}\right)p\right\}\cdot d\theta dz\,. \tag{2.5}$$

Moreover, the computation is sometimes simplified by using "Shelly's Method", which assumes a functional dependence of the pressure in the axial direction [11,14]:

$$p(\theta,z)=P_\theta\left[1-\left|\frac{2z}{L}\right|^n\right]. \tag{2.6}$$

Here, n is a chosen constant which depends on the length-to-diameter ratio of the bearing[6], and $-\frac{L}{2}\le z\le\frac{L}{2}$.

3 Fixed Pad Dynamic Coefficients

The calculation of dynamic coefficients for plain and fixed pad journal bearings is considered in this section. The calculation for the tilting pad bearing builds upon the fixed pad method, as presented in Section 4.

3.1 Journal Load Capacity

Once the pressure distribution is determined using one of the methods described in Section 2, the external load that can be supported by the journal is determined by integrating the pressure distribution over the film surface [5,13,16]:

$$\left.\begin{matrix}F_x\\F_y\end{matrix}\right\}=-\int_{-\frac{L}{2}}^{\frac{L}{2}}\int_{\theta_1}^{\theta_2}p\cdot\left\{\begin{matrix}\cos\theta\\\sin\theta\end{matrix}\right\}Rd\theta dz\,, \tag{3.1}$$

where F_x is the load in the x-direction, and F_y is the load in the y-direction (see the coordinate system in Figure 2.1 or Figure 2.2). The integration limits for Equation 3.1 correspond to the beginning of (θ_1) and the end of (θ_2) the active film region since the pressures are zero elsewhere when the boundary conditions described in Section 2.2 are applied.[7] Integrating over the entire film yields the net load that can be supported by the journal at the specified operating conditions for which the pressure field was computed. The force due to a portion of the overall film is computed in a similar manner, but with integration limits specific to the region of interest.

3.2 Perturbation Method for Computing Dynamic Coefficients

The reaction forces computed in Equation 3.1 can be related to dynamic stiffness and damping coefficients by expanding these forces about the static offset position (i.e., the normal operating point) using a Taylor's series expansion [5,13]:

---

[6] For medium-length journal bearings where ¼ ≤ L/D ≤ 1, n = 2 provides reasonable accuracy [11,14].

[7] θ_1 and θ_2 are limited to $\phi\le\theta\le(\phi+\pi)$ for a plain journal bearing based on the converging film region.

$$F_x = F_{x_0} + k_{xx}\Delta x + k_{xy}\Delta y + b_{xx}\Delta\dot{x} + b_{xy}\Delta\dot{y}$$
$$F_y = F_{y_0} + k_{yx}\Delta x + k_{yy}\Delta y + b_{yx}\Delta\dot{x} + b_{yy}\Delta\dot{y}\,, \tag{3.2}$$

where F_{x_0} is the x-component of the static load, F_{y_0} is the y-component of the static load, Δx and Δy are small amplitude motions in the x- and y-directions, respectively, and $\Delta\dot{x}$ and $\Delta\dot{y}$ are the vibration velocities in the x- and y-directions, respectively. The coefficients of the Δx, Δy, $\Delta\dot{x}$, and $\Delta\dot{y}$ terms in Equation 3.2 constitute the equivalent bearing dynamic coefficients used for dynamic analyses [5]. These coefficients are determined by solving the Reynolds equation using a perturbation on the film thickness, Δh, such that [5,7]:

$$h = h_0 + \Delta h, \tag{3.3}$$

where

$$h_0 = \text{nominal film thickness} = c + x_0\cdot\cos\theta + y_0\cdot\sin\theta, \tag{3.4}$$

$$\Delta h = \text{perturbed film thickness} = \Delta x\cdot\cos(\theta) + \Delta y\cdot\sin(\theta), \text{ and} \tag{3.5}$$

$$\frac{\partial h}{\partial t} = \Delta\dot{x}\cos\theta + \Delta\dot{y}\sin\theta\,. \tag{3.6}$$

The perturbed film thickness creates a perturbed film pressure that is defined using a Taylor's series expansion [5,8,16,23]:

$$p = p_0 + p_x\Delta x + p_y\Delta y + p'_x\Delta\dot{x} + p'_y\Delta\dot{y} = p_0 + \Delta p, \tag{3.7}$$

where p_x and p_y are the pressure components related to the film stiffness and p'_x and p'_y are the pressure components related to the film damping.

Substituting Equations 3.3 to 3.7 into Equation 2.1 and retaining first order terms only yields five equations (coefficients of Δx, Δy, $\Delta\dot{x}$, and $\Delta\dot{y}$ are equated in this step):

$$\begin{aligned}
Z\{p_0\} &= \frac{1}{2}\Omega\frac{\partial h}{\partial\theta} \\
Z\{p_x\} &= -3\frac{\cos\theta}{h_0}\frac{1}{2}\Omega\frac{\partial h_0}{\partial\theta} - 3\frac{h_0^3}{12\mu}\frac{1}{R}\frac{\partial p_0}{\partial\theta}\frac{1}{R}\frac{\partial}{\partial\theta}\left(\frac{\cos\theta}{h_0}\right) - \frac{1}{2}\Omega\sin\theta \\
Z\{p_y\} &= -3\frac{\sin\theta}{h_0}\frac{1}{2}\Omega\frac{\partial h_0}{\partial\theta} - 3\frac{h_0^3}{12\mu}\frac{1}{R}\frac{\partial p_0}{\partial\theta}\frac{1}{R}\frac{\partial}{\partial\theta}\left(\frac{\sin\theta}{h_0}\right) - \frac{1}{2}\Omega\cos\theta \\
Z\{p'_x\} &= \cos\theta \\
Z\{p'_y\} &= \sin\theta
\end{aligned} \tag{3.8}$$

where the left hand operator $Z\{\}$ is defined as:

$$Z\{\ \} = \frac{1}{R}\frac{\partial}{\partial\theta}\left(\frac{h_0^3}{12\mu}\frac{1}{R}\frac{\partial}{\partial\theta}\right) + \frac{\partial}{\partial z}\left(\frac{h_0^3}{12\mu}\frac{\partial}{\partial z}\right) \tag{3.9}$$

By combining Equations 3.1, 3.2, and 3.7 we have:

$$\begin{aligned}
\begin{Bmatrix} k_{xx} \\ k_{yx} \end{Bmatrix} &= -\int_{-\frac{L}{2}}^{\frac{L}{2}}\int_{\theta_1}^{\theta_2} p_x \cdot \begin{Bmatrix} \cos\theta \\ \sin\theta \end{Bmatrix} R\,d\theta\,dz \\
\begin{Bmatrix} k_{xy} \\ k_{yy} \end{Bmatrix} &= -\int_{-\frac{L}{2}}^{\frac{L}{2}}\int_{\theta_1}^{\theta_2} p_y \cdot \begin{Bmatrix} \cos\theta \\ \sin\theta \end{Bmatrix} R\,d\theta\,dz \\
\begin{Bmatrix} b_{xx} \\ b_{yx} \end{Bmatrix} &= -\int_{-\frac{L}{2}}^{\frac{L}{2}}\int_{\theta_1}^{\theta_2} p'_x \cdot \begin{Bmatrix} \cos\theta \\ \sin\theta \end{Bmatrix} R\,d\theta\,dz \\
\begin{Bmatrix} b_{xy} \\ b_{yy} \end{Bmatrix} &= -\int_{-\frac{L}{2}}^{\frac{L}{2}}\int_{\theta_1}^{\theta_2} p'_y \cdot \begin{Bmatrix} \cos\theta \\ \sin\theta \end{Bmatrix} R\,d\theta\,dz
\end{aligned} \tag{3.10}$$

Integration over the entire film surface in Equation 3.10 yields the dynamic coefficients that are often used in rotor dynamic analyses. For high order structural finite element analyses, *these coefficients can be distributed along the journal circumference by specifying appropriate integration limits corresponding to the finite element node locations.* It must be noted, however, that the distributed bearing coefficients *do not* account for changes in the film that result from flexure of either the journal or bearing, and thus this method is only an approximation for cases when the journal and/or bearing are flexible. See Reference 23 for a discussion of the effect of such flexibility on the dynamic coefficients.

4 Tilting Pad Dynamic Coefficients

Computation of dynamic coefficients for the tilting pad bearing is more involved than what is presented in the previous section for the 'fixed pad' bearings. The method presented below for tilting pad bearings builds upon the methods described above.

4.1 Tilting Pad Characteristics

A tilting pad bearing is composed of N pads, each with the capability of pivoting around a fictitious point located on a circle called the *pivot circle*. The main parameters include (see Figure 2.2): the number of pads, N; the journal radius, R; the pivot point circle clearance, C'; the pad angle, γ; equivalent mass of the pad, $M = I/R^2$; pivot location, ψ; pivot pad location ratio, α/γ; pad width, L; pad radius of curvature, R_p; and the machined clearance, $C = R_p - R$.

The preload[8], also referred to as the preset, is an important analysis parameter for the tilting pad bearing. The preload is a measure of the converging film that is created by the bearing geometry and not by an external load as the name might infer. Extreme bearing preloads are shown in Figure 4.1 to aide in the visualization of this parameter.

[8] Note that the preload, $m = 1 - C'/C$, is different from the preload ratio, C'/C.

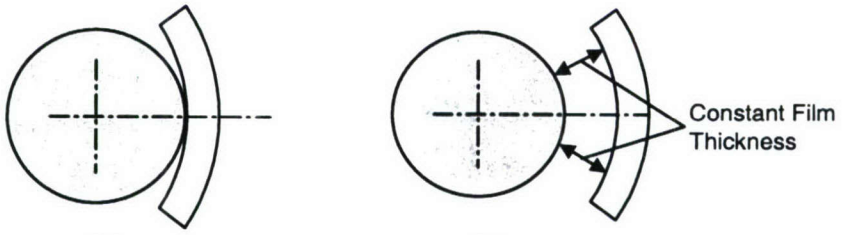

(a) (b)

Figure 4.1. Concept of bearing preload: (a) preload = 1 (preload ratio = 0), (b) preload = 0.

An important characteristic of the tilting pad bearing that separates it from the other types of bearings is the existence of a rotational degree of freedom for each pad. These additional degrees of freedom result in a total of 4+5*N* stiffness and 4+5*N* damping coefficients [11]. Because rotor dynamic models generally are not concerned with modeling the motion of the individual pads, methods have been developed to obtain a *reduced* set of coefficients (4 stiffness and 4 damping) by assuming a vibration frequency for the pad rotation. A discussion of reduced coefficients is provided below in Section 4.3. Prior to performing any type of dynamic coefficient reduction, however, the static characteristics must be defined.

4.2 Pad Assembly Method

The procedure for computing tilting pad dynamic coefficients begins with determining static characteristics of each tilting pad operating as a fixed pad. The characteristics of interest are the force and journal eccentricity. Once the static characteristics are known for a single fixed pad, the static characteristics of the tilting pad bearing are determined using superposition of the fixed pad results. This method, originally introduced by Lund [13] and used by other researchers in subsequent studies [20,21,22], is know as the *Pad Assembly Technique*. The local eccentricity, ε_i, and attitude angle, ϕ_i, of each pad is determined using Equation 4.1.

$$\varepsilon_i \cos\phi_i = m - \varepsilon_0 \cos(\psi_i - \phi_0), \tag{4.1}$$

where ε_i is the eccentricity ratio relative to pad i, ϕ_i is the attitude angle relative to pad i, ε_0 is the eccentricity ratio of the assembled bearing, and ϕ_0 is the attitude angle of the assembled bearing relative to the global coordinate system (see Figure 4.2).

Equation 4.1 is derived from geometrical considerations using a local pad coordinate system as shown in Figure 4.2 [13]. This assembly method generally involves a trial and error approach to find the assembled journal eccentricity and attitude angle (see Figure 2.1) such that the journal load equals the applied load. Often, a Newton-Raphson based iteration scheme is employed during this step [20].

Once the bearing is assembled, the dynamic coefficients for each pad are determined by applying the methods presented in Section 2.3 using the eccentricity and attitude angle relative to each pad in the pad's local coordinate system. The dynamic coefficients for each pad are computed in the local pad coordinate system (see Figure 4.2) assuming the pad is fixed (i.e., not free to rotate about its pivot point). However, because of the pad rotational degree of freedom, there is no

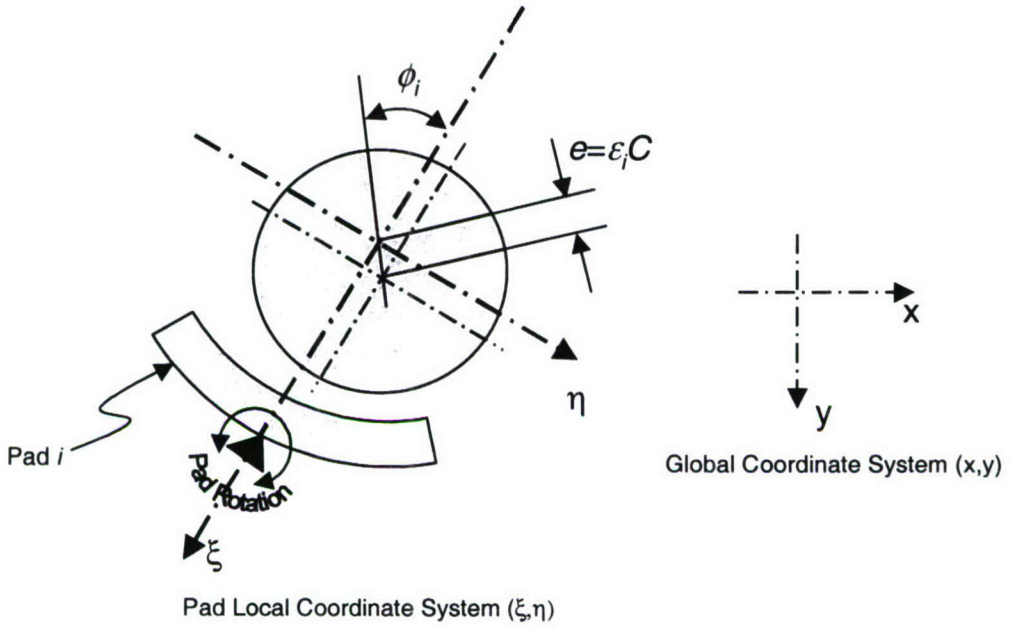

Figure 4.2. Tilting pad local and global coordinate systems.

static force in the η-direction and the dynamic force in this direction is a function of the pad's rotational effect on the fluid film as well as its inertia and vibration frequency.

4.3 Synchronous Reduction of Dynamic Coefficients

At this point, an assumption of the pad vibration frequency is often made and the coefficients are reduced from 8+10*N* to 8 (4 stiffness and 4 damping) coefficients so they can be incorporated into a low-order structural model. The most commonly used assumption is that of synchronous vibration of the pads with the rotational speed of the journal, which is often referred to as the *synchronous reduction* of the dynamic coefficients. This method was originally proposed by Lund [13]. The pertinent equations are as follows (Additional details can be found in References 11 and 13.):

$$
\begin{aligned}
k_{xx} &= k'_{\xi\xi}\cos^2\psi + k'_{\eta\eta}\sin^2\psi - \left(k'_{\xi\eta} + k'_{\eta\xi}\right)\cos\psi\sin\psi \\
k_{xy} &= k'_{\xi\eta}\cos^2\psi - k'_{\eta\xi}\sin^2\psi + \left(k'_{\xi\xi} - k'_{\eta\eta}\right)\cos\psi\sin\psi \\
k_{yx} &= k'_{\eta\xi}\cos^2\psi - k'_{\xi\eta}\sin^2\psi + \left(k'_{\xi\xi} - k'_{\eta\eta}\right)\cos\psi\sin\psi \\
k_{yy} &= k'_{\eta\eta}\cos^2\psi + k'_{\xi\xi}\sin^2\psi + \left(k'_{\xi\eta} + k'_{\eta\xi}\right)\cos\psi\sin\psi \\
\omega b_{xx} &= \omega b'_{\xi\xi}\cos^2\psi + \omega b'_{\eta\eta}\sin^2\psi - \left(\omega b'_{\xi\eta} + \omega b'_{\eta\xi}\right)\cos\psi\sin\psi \\
\omega b_{xy} &= \omega b'_{\xi\eta}\cos^2\psi - \omega b'_{\eta\xi}\sin^2\psi + \left(\omega b'_{\xi\xi} - \omega b'_{\eta\eta}\right)\cos\psi\sin\psi \\
\omega b_{yx} &= \omega b'_{\eta\xi}\cos^2\psi - \omega b'_{\xi\eta}\sin^2\psi + \left(\omega b'_{\xi\xi} - \omega b'_{\eta\eta}\right)\cos\psi\sin\psi \\
\omega b_{yy} &= \omega b'_{\eta\eta}\cos^2\psi + \omega b'_{\xi\xi}\sin^2\psi + \left(\omega b'_{\xi\eta} + \omega b'_{\eta\xi}\right)\cos\psi\sin\psi
\end{aligned}
\qquad (4.2)
$$

where

$$
\begin{aligned}
k'_{\xi\xi} &= k_{\xi\xi} - \left(pk_{\xi\eta} + q\varpi b_{\xi\eta}\right)k_{\eta\xi} - \left(qk_{\xi\eta} - p\varpi b_{\xi\eta}\right)\varpi b_{\eta\xi} \\
k'_{\xi\eta} &= -M\varpi^2\left(pk_{\xi\eta} + q\varpi b_{\xi\eta}\right) \\
k'_{\eta\xi} &= -M\varpi^2\left(pk_{\eta\xi} + q\varpi b_{\eta\xi}\right) \\
k'_{\eta\eta} &= -M\varpi^2\left(1 + pM\varpi^2\right) \\
\varpi b'_{\xi\xi} &= \varpi b_{\xi\xi} - \left(pk_{\xi\eta} + q\varpi b_{\xi\eta}\right)\varpi b_{\eta\xi} + \left(qk_{\xi\eta} - p\varpi b_{\xi\eta}\right)k_{\eta\xi} \\
\varpi b'_{\xi\eta} &= M\varpi^2\left(qk_{\xi\eta} - p\varpi b_{\xi\eta}\right) \\
\varpi b'_{\eta\xi} &= M\varpi^2\left(qk_{\eta\xi} - p\varpi b_{\eta\xi}\right) \\
\varpi b'_{\eta\eta} &= \left(M\varpi^2\right)^2 q
\end{aligned}
\qquad (4.3)
$$

and

$$
\begin{aligned}
p &= \frac{k_{\eta\eta} - M\varpi^2}{\left(k_{\eta\eta} - M\varpi^2\right)^2 + \left(\varpi b_{\eta\eta}\right)^2} \\
q &= \frac{\varpi b_{\eta\eta}}{\left(k_{\eta\eta} - M\varpi^2\right)^2 + \left(\varpi b_{\eta\eta}\right)^2}
\end{aligned}
\qquad (4.4)
$$

The process of reducing these coefficients in this manner introduces a frequency dependence of the coefficients as shown in Equation 4.3.

4.4 Coefficients for Explicitly Modeled Tilting Pads

To avoid the complications associated with using reduced coefficients (i.e., frequency dependent coefficients and no formal method to circumferentially distribute the coefficients for a high-order structural model), the pads can be modeled explicitly in a finite element model and the rotor and stator can be coupled through the pads using distributed dynamic coefficients. The coefficient distribution is accomplished through the application of appropriate integration limits in Equation 3.10. With this approach, the pad rotational degrees of freedom are accounted for in the finite element model and the coefficients are not frequency dependent[9]. Note that the coefficients are computed in a local coordinate system and then transformed to the global coordinate system using a transformation matrix, T, such that $K = [T]^T[k][T]$ and $B = [T]^T[b][T]$, where K and B are the coefficients in the global coordinate system, and k and b are the coefficients in the local coordinate system. The transformation matrix, T, is defined such that $\vec{r} = T\underline{\vec{r}}$ where $\underline{\vec{r}}$ is a displacement in the global coordinate system and $\vec{r}$ a displacement in the local coordinate system [25]. For the coordinate systems defined herein (i.e., angles measured

[9] Note that the coefficients are a function of the journal rotation rate because this has an effect on the fluid film pressure characteristics. However, for a given journal speed, Ω, all of the journal bearing dynamic coefficients, except for the tilting pad reduced coefficients, are independent of vibration frequency.

from the negative x-direction), the transformation matrix is computed as follows for each pad coordinate system:

$$T_i = \begin{bmatrix} -\cos\psi_i & -\sin\psi_i \\ \sin\psi_i & -\cos\psi_i \end{bmatrix}, i = 1 \text{ to } N. \tag{4.5}$$

When computing the dynamic coefficients for a tilting pad bearing, it is important to recognize that the final results are a function of the bearing load, direction of applied load (e.g., load-on-pad versus load-between-pads), journal operating speed, as well as the other fluid film parameters defined above. Additional effects on the computed equivalent bearing coefficients such as those caused by a non-rigid pivot and a flexible pad have not been addressed here but are discussed in the literature [23,24]. Note that pads for which there is no converging film, called *unloaded pads*, generally do not contribute to the overall stiffness but do in some cases (depending on their pivot design) contribute to the damping [22].

4.5 Application of Dynamic Coefficients to Finite Element Structural Models

The unsymmetric bearing stiffness matrices that often result for bearing models can be difficult to implement in structural finite element models. The presence of an unsymmetric matrix causes the system to have complex eigenvalues, and thus a complex eigensolution may be required. Standard methods for incorporating such matrices into a finite element code are available. For instance, the direct matrix input cards (DMIG) of COSMIC/, MSC/ and CSA/ Nastran can be used to implement any type of mass, stiffness, or damping matrix (symmetric or unsymmetric, real or complex) using the M2GG, K2GG, or B2GG case control commands for symmetric matrices—for all solution sequences—or the M2PP, K2PP, or B2PP case control commands for unsymmetric matrices—for dynamic response analyses only (excluding normal modes analyses). The reader is referred to Nastran documentation [26] for descriptions of these methods and their limitations. Note that the stiffness matrix can be decomposed into a symmetric matrix ($k_{sym} = \left(k + k^T\right)/2$) and an anti-symmetric matrix ($k_{antisym} = \left(k - k^T\right)/2$) such that $k=k_{sym}+k_{antisym}$. The symmetric matrix can be added using the K2GG case control command while the anti-symmetric matrix can be added using the K2PP case control command. Adding the matrix in this manner and performing a modal complex eigensolution (Nastran SOL 110) allows the effect of the anti-symmetric matrix to be evaluated in terms of resonance frequency changes from the normal modes solution to the complex eigensolution. If the effects are negligible, then dynamic results can be obtained using the symmetric matrix with no need for unsymmetric matrix solvers, which are generally more computationally expensive.

5 Distributed Coefficient Example Problem

An example problem is provided to illustrate the effect of applying bearing coefficients to a FE structural model using: 1) the method presented herein for distributed coefficients, and 2) a uniform coefficient distribution to represent a method that is often applied to such models. The example problem focuses on a tilting pad bearing design because of the complexity associated with this type of bearing.

As discussed above, the bearing pads of a tilting pad bearing are generally not explicitly modeled in a structural model. Instead, the bearing coefficients are computed using some sort of reduction technique (e.g., synchronous reduction) to account for the pad vibration about the rotational degrees of freedom and the coefficients (stiffness and damping) are applied to the bearing using an ad hoc distribution that may only capture the low-order bearing effects. For the example problem, the response of the model is computed twice: once with the proposed bearing coefficient distribution and the tilting pads explicitly modeled (the "actual coefficient model"), and a second time using a uniform[10] distribution of synchronously reduced coefficients to each node on the rotor circumference (the "reduced coefficient model"). The structure being modeled is shown in Figure 5.1 with relevant information shown in Figure 5.2. The outer ring and tilting pads are modeled using steel while the rotor ring is modeled using aluminum. The bearing consists of eight tilting pads that are equally spaced around the journal circumference and connected to the rotor ring at the pivot points shown in Figure 5.3 with a pad pivot location ratio, α/γ, of 0.5 (see Figure 2.2). Other details regarding the bearing are shown in Table 5.1:

Table 5.1. Bearing parameters (water at 305 K)

$\mu = 7.69\text{x}10^{-4}$ Pa·s	$\Omega = 19.2$ Hz	$\gamma = 32°$
$\rho = 995.$ kg/m^3	$L = 0.0203$ m	$\alpha/\gamma = 0.5$
$D = 0.323$ m	$C = 2.54\text{x}10^{-4}$ m	$m = 0.4$
$\psi = 180°$		

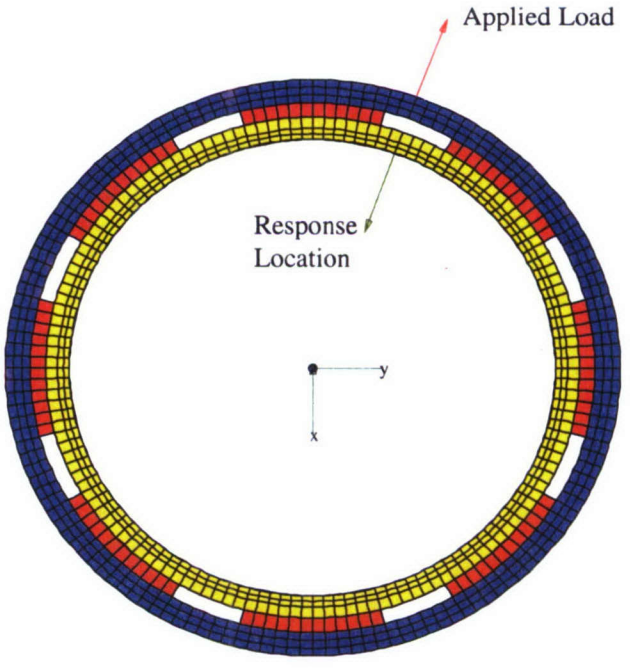

Figure 5.1. FE model for the actual coefficient model showing applied load and response locations.

[10] The uniform distribution chosen here has no physical basis, but is consistent with what might be employed for such a model.

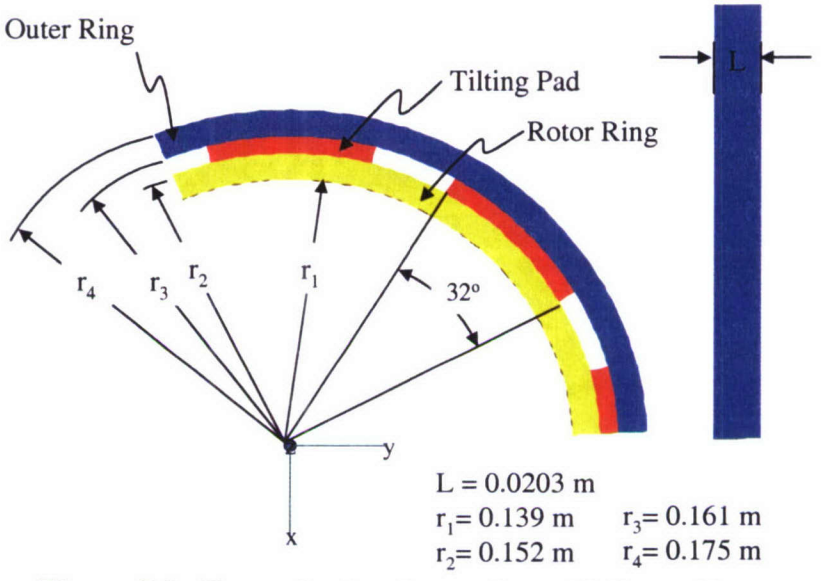

Figure 5.2. Example structure relevant information.

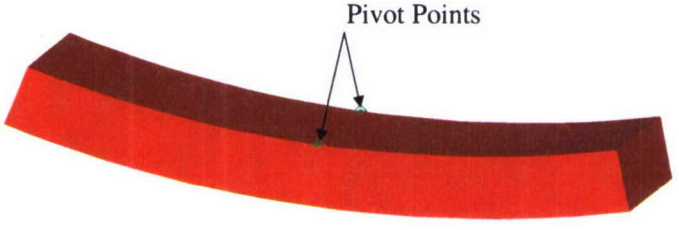

Figure 5.3. Tilting pad pivot location.

Because the tilting pads are not explicitly modeled when synchronously reduced coefficients are used, the model for the reduced coefficients must be slightly modified from what is shown in Figure 5.1. Two things should be noted regarding the changes. First, because the pads are connected to the rotor ring in the model shown in Figure 5.1, concentrated mass elements are added to the reduced coefficient model at the pivot locations to account for the translational inertia of the pads (the rotational inertia about the pad pivots is inherently accounted for in the synchronously reduced coefficients). These point masses are shown in Figure 5.4. The rotor and stator rings are identical for both models, and this fact enables direct comparisons between the results from each model.

The first step in the analysis is to compute the bearing dynamic coefficients. Two sets of coefficients are computed: one set of distributed coefficients using the methods presented here with a distribution to the FE grids on the tilting pads, and a second set using the method of synchronous reduction and a uniform distribution to the FE nodes on the journal circumference. In both cases, the bearing coefficients connect to the FE grids on the inner surface of the outer ring. Because the pad assembly method is employed here, both coefficient computations require the static operating characteristics (eccentricity and attitude angle) for each pad of the tilting pad bearing.

The pad static characteristics are determined by solving the Reynolds equation and computing the hydrodynamic force (Equation 3.1) for a variety of journal eccentricities. The attitude angle,

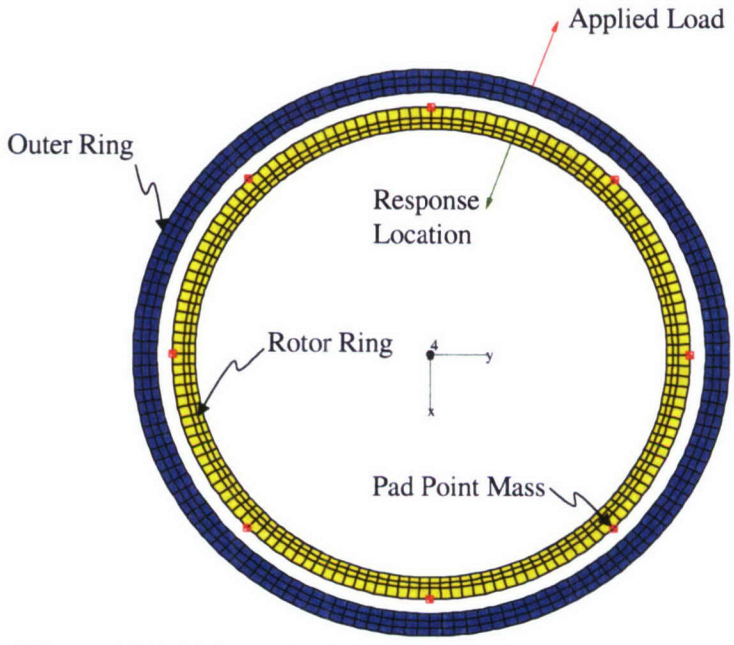

Figure 5.4. FE model for the reduced coefficient model.

ϕ, for each eccentricity is obtained by varying ϕ until the force in the η-direction is numerically zero (the coordinate system in Figure 4.2 is defined such that the load is entirely in the ξ-direction). A sample pressure field for a journal eccentricity ratio of 0.276 and an attitude angle of 52.2° is shown in Figure 5.5. The pressure field was computed using a finite difference approximation for the Reynolds equation with a discretization of 100 in the θ-direction and 60 in the z-direction. The Reynolds boundary conditions were applied using an ambient pressure of zero for all boundaries. The net journal load that can be supported by this pressure field is (computed from Equation 3.1): F_ξ = 0.371 N and F_η = -6.93×10^{-10} N. Performing such a calculation for several eccentricities yields the results shown in Figure 5.6.

The pad assembly method, described in Section 4.2, is then employed to compute the overall journal eccentricity and attitude angle to support a desired load of 111.0 N. In doing this, the local eccentricity and attitude angle relative to each pad is obtained and the bearing coefficients can then be computed for each pad. It is at this point where the two methods diverge. The synchronously reduced coefficients are computed using coefficients integrated over the entire pad surface and the methods described in Section 4.3 are employed, while the actual coefficient model uses a distribution of the coefficients to the pad FE grids. The coefficients are distributed by solving for the pressure field over each pad and choosing appropriate integration limits in Equation 3.10 based on the pad grid locations. The resulting coefficients for all pads are shown in Figure 5.7 for the stiffness and Figure 5.8 for the damping. As shown in these figures, the stiffness and damping are largest for the pad at 180° and decrease to zero for the unloaded pad at 0°. Based on these results, one can imagine the errors that would be associated with a uniform distribution of these coefficients over the journal circumference.

Because the reduced coefficients incorporate the effects of the pad rotation, an equivalent pad mass is required for the reduced coefficient computation. The pad mass is computed as follows for the steel pads:

$$M = \frac{I}{R_p^2} = \frac{6.53x10^{-6}\,kg \cdot m^2}{(0.165kg)^2} = 2.50x10^{-4}\,kg\,. \tag{5.1}$$

The resulting coefficients after performing the reduction are shown in Table 5.2. These coefficients are equally distributed to the FE grids on the journal circumference of the reduced coefficient model.

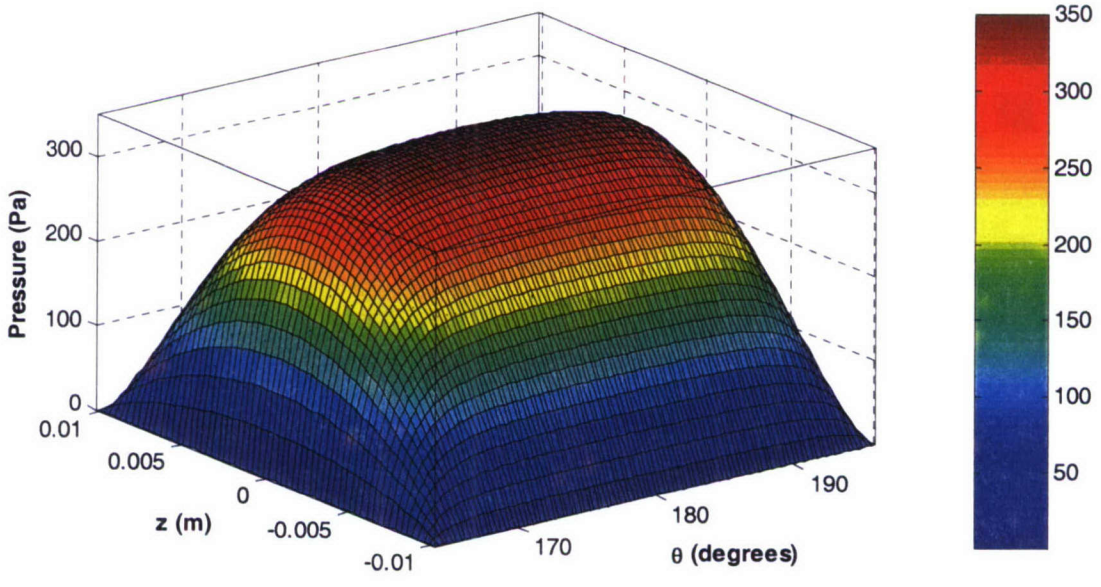

Figure 5.5. Sample pressure field for ε=0.276 and ϕ=52.2°.

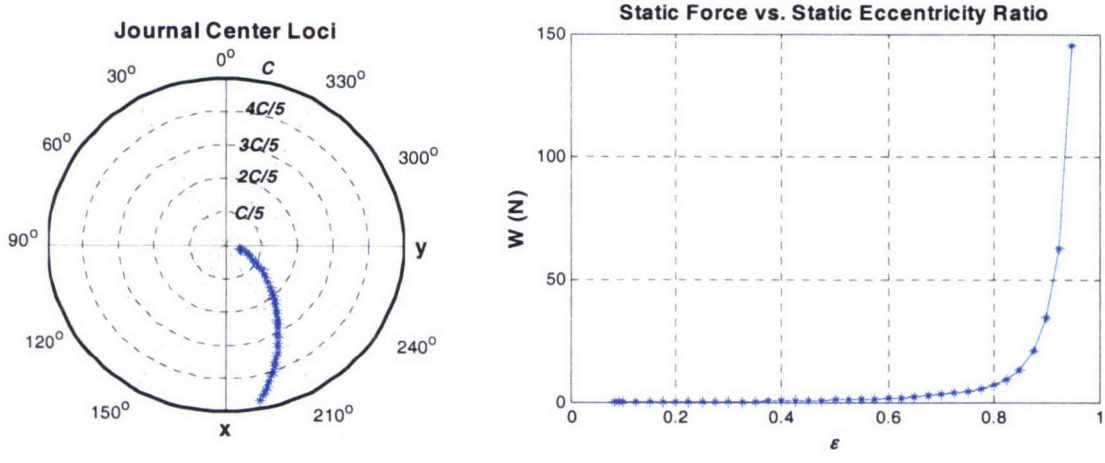

Figure 5.6. Sample fixed pad static characteristics (W = journal load).

Table 5.2. Synchronously reduced coefficients.

$k_{xx} = 9.71 \times 10^6$ N/m	$k_{xy} = -77.8$ N/m
$k_{yx} = 132.$ N/m	$k_{yy} = 3.36 \times 10^5$ N/m
$b_{xx} = 1.98 \times 10^4$ N/(m·s)	$b_{xy} = 0.797$ N/(m·s)
$b_{yx} = -1.19$ N/(m·s)	$b_{yy} = 1.54 \times 10^3$ N/(m·s)

It is interesting to note that it is the inclusion of the pad equivalent mass in this calculation that causes the cross coefficients to become non-zero. Performing the same computation with no pad mass yields zero cross coefficients as shown in Table 5.3. The pad mass does have an effect on all of the coefficients in these tables, but the differences are small relative to the diagonal terms (i.e., k_{xx}, k_{yy}, b_{xx}, and b_{yy}).

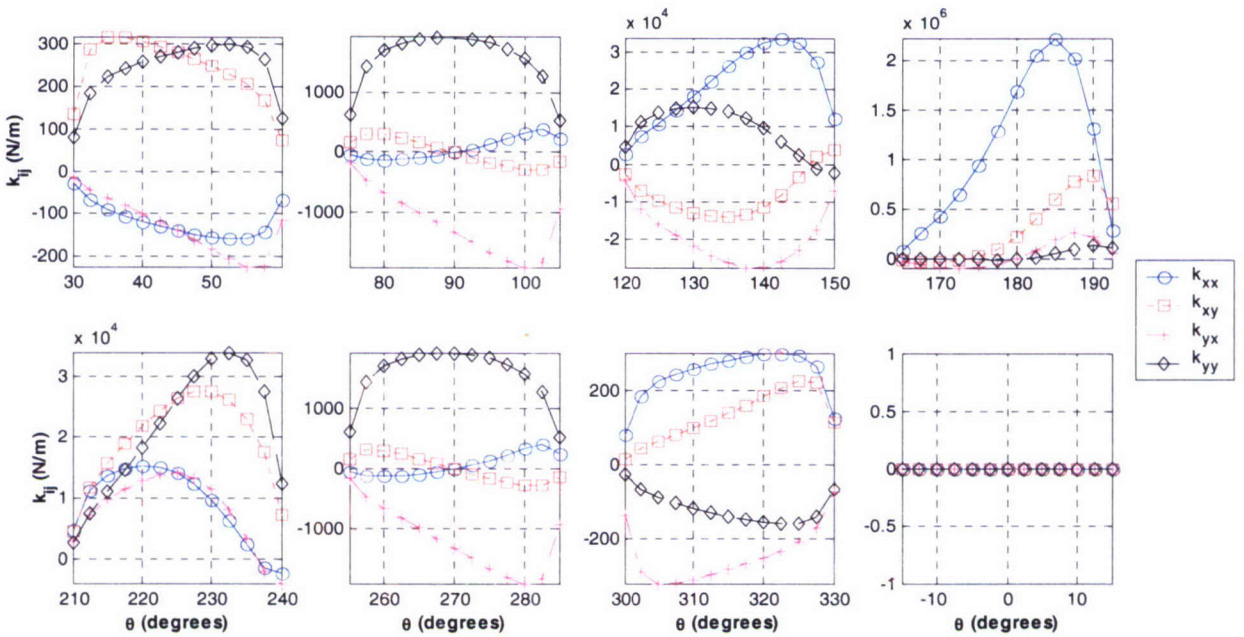

Figure 5.7. Distributed stiffness coefficients for the actual coefficient model.

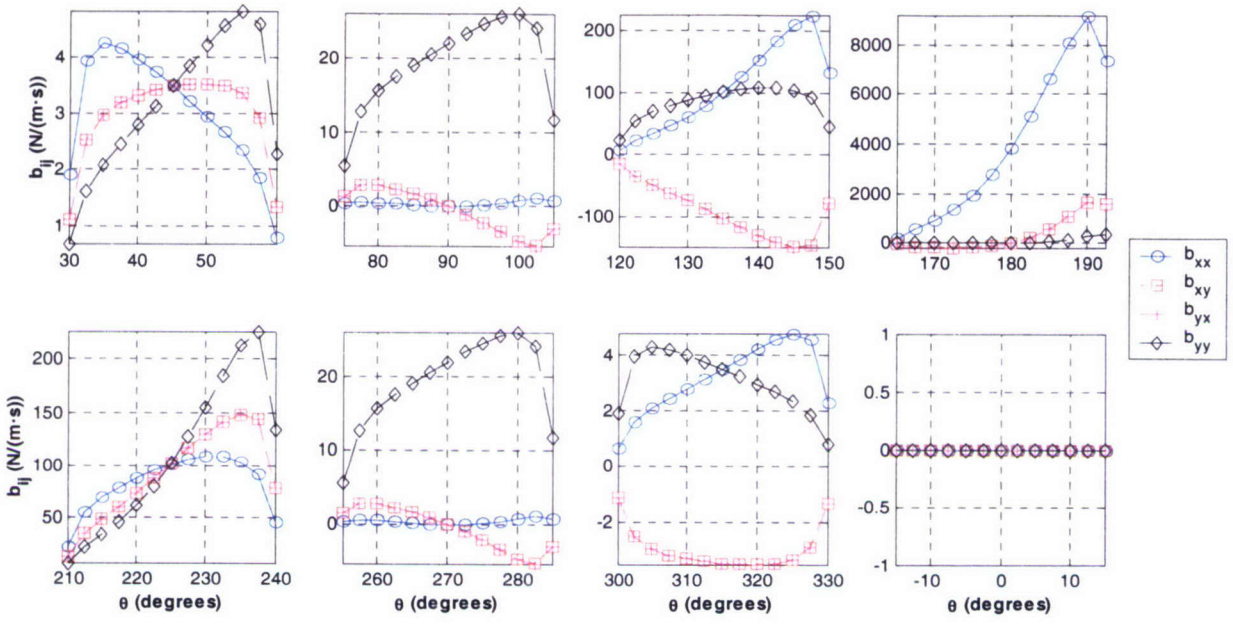

Figure 5.8. Distributed damping coefficients for the actual coefficient model.

Table 5.3. Synchronously reduced coefficients using no pad mass.

$k_{xx} = 9.71 \times 10^6$ N/m	$k_{xy} = 0$
$k_{yx} = 0$	$k_{yy} = 3.36 \times 10^5$ N/m
$b_{xx} = 1.98 \times 10^4$ N/(m·s)	$b_{xy} = 0$
$b_{yx} = 0$	$b_{yy} = 1.54 \times 10^3$ N/(m·s)

Also note that the pad located at $\psi = 0$ is unloaded for this bearing and thus does not contribute to the bearing coefficients (but the damping could contribute depending on the pivot design). If this pad were fully loaded (i.e., a converging film over the entire surface), its contribution would cause the direct coefficients in Table 5.2 and Table 5.3 to be equal because of the bearing symmetry (i.e., k_{xx}=k_{yy}, and b_{xx}=b_{yy}).

Accelerance (acceleration/force) transfer function plots for a radial excitation on the outer ring and a response location on the rotor (see Figure 5.1 and Figure 5.4) are shown in Figure 5.9 for both models. These results were obtained by performing a frequency response analysis using MSC/Nastran with the bearing coefficients added via DMIG cards [26]. As can be seen in this figure, the transfer accelerances have similar characteristics but exhibit differences in both amplitude and resonance content for the two models. These differences reflect the method by which the bearing coefficients are applied since the models are otherwise identical. The mean accelerance (response points averaged over the rotor inner surface) and corresponding circumferential Fourier decomposition for each model due to the same drive point as before is shown in Figure 5.10. These plots show a significant amount of cross modal coupling for the actual coefficient model relative to the reduced coefficient model for the resonances near 300

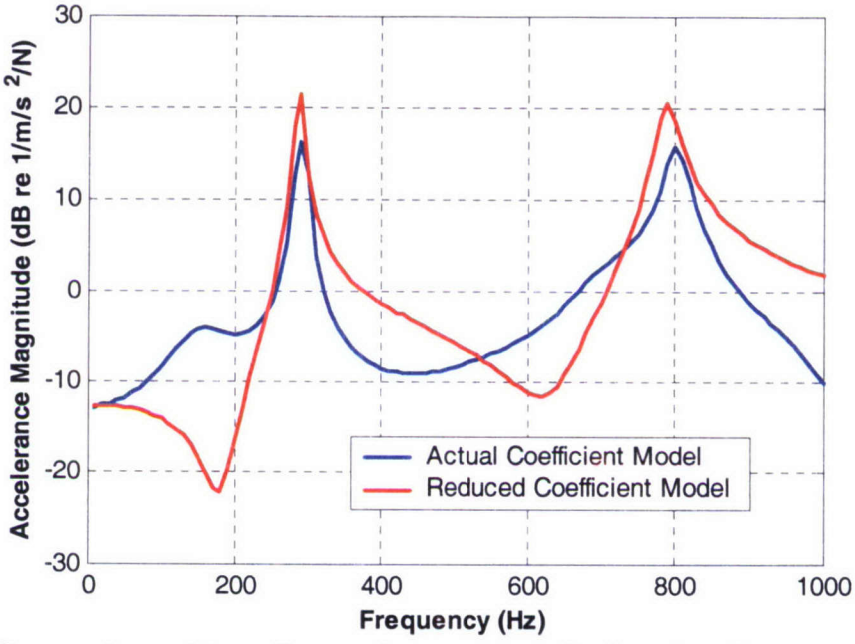

Figure 5.9. Comparison of transfer accelerance magnitude using the proposed coefficient distribution and a uniform distribution of synchronously reduced coefficients.

and 800 Hz. The Fourier decomposed results are obtained using the discrete Fourier transform (DFT) applied along the circumferential direction for each frequency as follows [27]:

$$\bar{a}[\nu] = \frac{1}{NNS}\sum_{i=1}^{NNS}\frac{1}{N}\sum_{\mu=0}^{N-1} a[i,\mu]e^{-i\left(\frac{2\pi}{N}\right)\mu\nu}, \tag{5.2}$$

where $\bar{a}[\nu]$ is the average accelerance at a specific frequency for the Fourier component ν, NNS is the number of nodes per segment of the structure (the structure is divided into N equal segments along the circumferential direction), and $a[i,\mu]$ is the accelerance at node i of segment μ. Because only the first $N/2$ Fourier components can be resolved for an N-point DFT and these coefficients are "mirrored" about N/2, the mirrored coefficients are summed together such that $\bar{a}[1]$ = abs($\bar{a}[1]$) + abs($\bar{a}[N-1]$), $\bar{a}[2]$ = abs($\bar{a}[2]$) + abs($\bar{a}[N-2]$), etc. to ensure the decomposed results sum together to yield the overall response. Note that if N is an even number, the $\bar{a}[N/2]$ component is not mirrored. Here, N is chosen to be eight based on the structure having eight times symmetry, which is a result of having eight tilting pads equally spaced around the rotor circumference. This choice of N for the reduced coefficient model is sufficient to resolve all of the Fourier components because the structure is axi-symmetric with eight times symmetry. The actual coefficient model is not axi-symmetric due to the presence of a non-uniform bearing coefficient distribution. Thus, a larger value of N should be chosen for the actual coefficient model to decompose the response with minimal aliasing effects. However, the

choice of N=8 is sufficient for both models to show the effect of the bearing distribution method on the Fourier content[11] (see Figure 5.10).

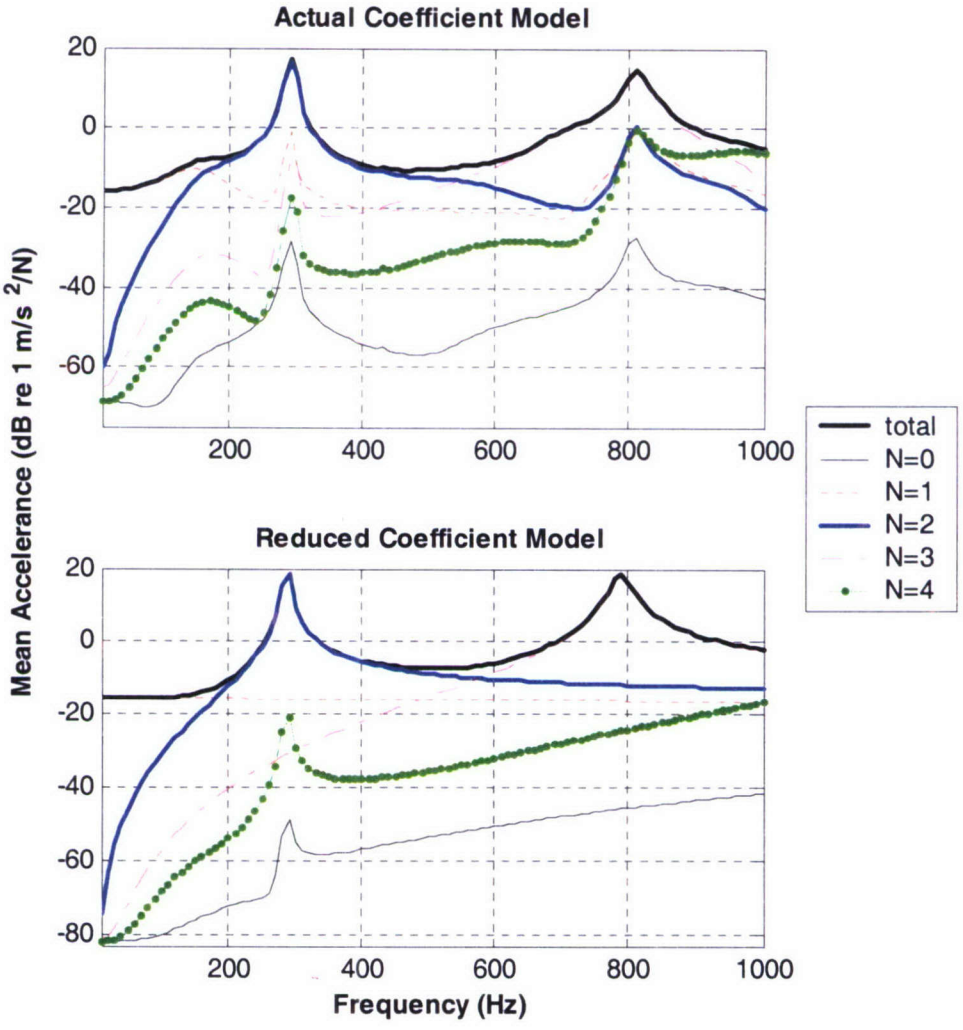

Figure 5.10. Mean rotor accelerance decomposition into circumferential Fourier components.

A summary of resonance frequencies and structural damping loss factors for the two models is provided in Table 5.4 for resonances up to 1 kHz. Several aspects of these results should be noted. First, numerous modes are overdamped due to the presence of the bearing damping, and thus do not appear in this table. Second, several modes have a damping consistent with the assumed material damping of 0.001 (e.g., 298., 429., and 818. Hz for the actual coefficient model, and 310., 429., and 874. Hz for the reduced coefficient model). These are torsional modes, indicated by a "T" in Table 5.4, that are not affected by the bearing coefficients because the coefficients act only in the radial direction and the centerline rotor and outer ring grids where the bearing coefficients are applied have displacements only in the axial direction for these

[11] An evaluation using various values for N for the actual coefficient model decomposition has shown that aliasing effects have a negligible impact on the results reported in Figure 5.10.

modes. The differences between the resonance frequencies of each model for these modes are a result of neglecting the pad rotational inertia about the r and θ directions in the reduced coefficient model. Third, modes for which the rotor is spatially comprised of a single circumferential Fourier component are identified in this table with the variable "N" (bending modes only). Modes without such a designation are largely affected by the non-uniform coefficient distribution and are thus comprised of multiple Fourier components, which are not shown in the table. Next, resonances corresponding to the peaks in Figure 5.9 are shown in bold face font in Table 5.4. For these modes, both the rotor and outer ring are comprised of the same Fourier component shown in the table. Moreover, it is apparent from the damping in this table that the peak height near 800 Hz in Figure 5.9 is not due to disparate damping levels, but due to structural dissimilarities (the transfer accelerance peak and loss factor for the reduced coefficient model are both higher than those for the actual coefficient model). Finally, numerous repeated

Table 5.4. Resonance frequencies and damping levels.

Actual Coefficient Model		**Reduced Coefficient Model**	
Resonance Frequency (Hz)	**Loss Factor**	**Resonance Frequency (Hz)**	**Loss Factor**
3.72 (N=1)	16.		
7.72 (N=1)	6.0		
19.5 (N=1)	6.7		
153.	0.62		
		169. (N=2,x2)	2.1
261. (N=2)	0.068		
267. (N=2)	0.73		
288. (N=2)	**0.022**	**286. (N=2,x2)**	**0.018**
		287. (N=2,x2)	0.016
298. (T,x2)	0.001	310. (T,x2)	0.001
298. (N=2)	0.026		
299. (N=2)	0.022		
429. (T,x2) (outer ring)	0.001	429. (T,x2) (outer ring)	0.001
548.	0.48		
615.	0.54		
696. (N=3)	0.18		
746. (N=3)	0.27		
747.	0.62		
		788. (N=3)	0.031
809. (N=3)	**0.025**	**794. (N=3)**	**0.044**
		798. (N=3)	0.041
816.	0.053		
818. (T,x2)	0.001	874. (T,x2)	0.001
913.	0.42		
976.	0.22		

resonances occur for the reduced coefficient model due to the model's uniform bearing coefficient distribution and the structure's axi-symmetry (these are indicated by a "x2" next to the resonance frequencies in Table 5.4). Repeated resonances are also present in the actual coefficient model, but only for modes not affected by the non-uniformly distributed bearing coefficients (i.e., the torsional modes described previously).

6 Summary and Conclusions

A review of methods currently employed for modeling static and dynamic characteristics of fluid film bearings has been provided. Pertinent literature has been reviewed and summarized with an effort placed on highlighting the nuances associated with such models. In nearly all cases, the literature discusses the use of dynamic coefficients for rotor-dynamics models, in which a single stiffness and damping matrix is used to connect an individual rotor node to an individual stator/bearing node. The focus of this work was on developing dynamic coefficients for a structural finite element model, which uses a distribution of the coefficients over the journal circumference. The proposed method is applicable to all fluid film bearings. The method is approximate in the sense that the effect of a flexible journal and/or bearing is not incorporated in the resulting coefficients.

For the case of a tilting pad bearing, rotor-dynamics models often use a reduced set of coefficients such that the individual pads need not be modeled. The process of reducing the coefficients causes them to become frequency dependent since a frequency for the pad rotational degrees of freedom must be assumed. As discussed herein, by explicitly modeling the pads in, for example, a structural finite element model, the pad rotational degrees of freedom are accounted for in the finite element model and thus the bearing coefficients are no longer frequency dependent.

A brief discussion regarding the application of the computed dynamic coefficients for a structural finite element model is also provided. Because of the unsymmetric nature of the stiffness coefficients (the damping coefficient matrix should always be symmetric), there may be a need to directly input the matrices to the finite element model, depending on the available elements for the solver being used (e.g., ABAQUS, ANSYS, or NASTRAN). It was also suggested that symmetric and anti-symmetric matrices be created from the unsymmetric matrices to facilitate the solution process.

The importance of appropriately distributing the computed bearing coefficients is demonstrated through a numerical study wherein a comparison of results for a tilting pad bearing model are computed for two different implementations of the bearing coefficients. The two coefficient implementations are: 1) a synchronous reduction of the coefficients and a uniform distribution to the journal circumference in a model with no tilting pads, and 2) a model using the distribution method proposed herein which incorporates explicit structural models of the tilting pads and a distribution of the coefficients to each pad grid in the FE model. A comparison of results for these models shows substantial differences in the transfer accelerance (both in amplitude and circumferential makeup), resonance frequencies, and damping levels.

References

1. McDevitt, T. M., Campbell, R. L., Jenkins, D. L., Hambric, S. A., and Jonson, M. L., "Structural-Acoustic Issues Associated with Modeling Motor Noise Mechanisms," ARL Technical Memorandum No. 03-010.

2. Neale, M. J., editor, Bearings. Butterworth-Heinemann Ltd, Oxford, 1993.

3. Pinkus, O., "The Reynolds Centennial: A Brief History of the Theory of Hydrodynamic Lubrication," *Journal of Tribology*, Transactions of the ASME, **109**, January 1987, pp.

4. Norton, Robert L., Machine Design: An Integrated Approach. Prentice-Hall, NJ. 1996.

5. Lund, J. W., "Review of the Concept of Dynamic Coefficients for Fluid Film Journal Bearings." Journal of Tribology, **109**, January 1987, pp. 37-41.

6. Lund, J. W., "Evaluation of Stiffness and Damping Coefficients for Fluid-Film Bearings," Shock and Vibration Digest, **11**(1), 1979, pp. 5-10.

7. Chu, Chin, S. Wood, Kristin, L., and Busch-Vishniac, Ilene, J. "A Nonlinear Dynamic Model With Confidence Bounds for Hydrodynamic Bearings." Journal of Tribology, **120**, July 1998, pp. 595-604.

8. Constantinescu, V. N., *et al.*, Sliding Bearings. Allerton Press, Inc., New York, 1985.

9. Hirs, G. G., "A Bulk-Flow Theory for Turbulence in Lubricant Films," ASME Journal of Lubrication Technology, April 1973, pp. 137-146.

10. Szeri, A. Z., "Some Extensions of the Lubrication Theory of Osborne Reynolds," *Journal of Tribology*, Transactions of the ASME, 86-Trib-47, 1986, pp. 1-16.

11. White, M. F., and Chan, S. H., "The Subsynchronous Dynamic Behavior of Tilting-Pad Journal Bearings," *Journal of Tribology*, Transactions of the ASME, **114**, January 1992, pp. 167-173.

12. Chu, Chin, S. Wood, Kristin, L., and Busch-Vishniac, Ilene, J. "A Nonlinear Dynamic Model With Confidence Bounds for Hydrodynamic Bearings." Journal of Tribology, **120**, July 1998, pp. 595-604.

13. Lund, J. W., "Spring and Damping Coefficients for the Tilting-Pad Journal Bearing," *ASLE Transactions*, **7**, 1964, pp. 342-351.

14. Ettles, C. M., "The Analysis and Performance of Pivoted Pad Journal Bearings Considering Thermal and Elastic Effects," Journal of Lubrication Technology, Transactions of the ASME, **102**, pp. 182-192, 1980.

15. Someya, T. ed., Journal-Bearing Databook. Springer-Verlag Berlin, Heidelberg, 1989.

16. Dowson, D. editor, Hydrodynamic Lubrication: Bearings and Thrust Bearings. Elsevier Science, Amsterdam, The Netherlands, 1997.

17. Knight, J. D., and Barrett, L. E., "An Approximate Solution Technique for Multilobe Journal Bearings Including Thermal Effects, with Comparison to Experiment," *ASLE Transactions*, **26**(4), 1983, PP. 501-508.

18. Knight, J. D., and Barrett, L. E., "Analysis of Tilting Pad Journal Bearings with Heat Transfer Effects," *Journal of Tribology*, Transactions of the ASME, **110**, January 1988.

19. Ettles, C. M., "The Analysis and Performance of Pivoted Pad Journal Bearings Considering Thermal and Elastic Effects," Journal of Lubrication Technology, Transactions of the ASME, **102**, pp. 182-192, 1980.

20. Rouch, K. E., "Dynamics of Pivoted-Pad Journal Bearings, Including Pad Translation and Rotation Effects," *ASLE Transactions*, **26**, 1983, pp. 102-109.

21. Nicolas, J. C., Gunter, E. J., and Allaire, P. E., "Stiffness and Damping Coefficients for the Five-Pad Tilting-pad Bearing," *ASLE Transactions*, **22**(2), 1979, pp. 113-124.

22. Allaire, P. E., Parsell, J. K., and Barrett, L. E., "A Pad Perturbation Method for Tilting Pad Journal Bearing Dynamic Coefficients," Wear, **72**(1), pp. 29-44, January, 1981.

23. Lund, J. W., and Pedersen, L. B., "The Influence of Pad Flexibility on the Dynamic Coefficients of a Tilting Pad Journal Bearing," *Journal of Tribology*, Transactions of the ASME, **109**, pp. 65-70, January 1987.

24. Kirk, R. G., and Reedy, S. W., "Evaluation of Pivot Stiffness for Typical Tilting-Pad Journal Bearing Designs," *Journal of Vibration, Acoustics, Stress, and Reliability in Design*, Transactions of the ASME, **110**, pp. 165-171, April 1988.

25. Przemieniecki, J. S., Theory of Matrix Structural Analysis. Dover Publications Inc., New York, 1968, p. 67.

26. MSC/Nastran 2001 user's manual, MSC Software corporation.

27. Oppenheim, A. V. and Shafer, R. W., Discrete-Time Signal Processing, 2nd Edition, Prentice-Hall, Inc., New Jersey, 1999.

Appendix: Simplified Solutions to Reynolds Equation

Simplified solutions to Equation 2.1 are available for steady-state conditions (i.e., $\frac{\partial h}{\partial t} = 0$) for the case of an infinitely long plain journal bearing (i.e., $\frac{L}{D} \gg 1 \Rightarrow \frac{\partial}{\partial z} \ll \frac{\partial}{\partial \theta}$) and for the case of a short plain journal bearing (i.e., $\frac{L}{D} < 1 \Rightarrow \frac{\partial}{\partial \theta} \ll \frac{\partial}{\partial z}$). The solution to the long bearing approximation, called the *long bearing solution*, or the *Sommerfeld solution*, is shown in Equation A.1 [4].

$$p = \frac{\mu R \Omega}{C^2}\left[\frac{6\varepsilon \sin\gamma(2+\varepsilon\cos\gamma)}{(2+\varepsilon^2)\sqrt{1+\varepsilon^2}}\right] + p_a, \tag{A.1}$$

where C is the radial clearance, ε is the ratio of the eccentricity and the radial clearance (e/C), ϕ is the angle between the load direction and the film rupture location (see Figure 2.1), and p_a accounts for any supply pressure at $\gamma = \theta - \phi = 0$. Note that film rupture occurs at $\gamma = \pi$ and the active film falls within $0 \le \gamma \le \pi$. Equation A.1 predicts negative pressures for $\pi < \gamma < 0$, and thus the pressure is assumed to be p_a within this range. A relationship between the load and eccentricity is provided in Equation A.2.

$$W = \frac{\mu R^3 \Omega L}{c^2}\frac{12\pi\varepsilon}{(2+\varepsilon^2)\sqrt{1+\varepsilon^2}}, \tag{A.2}$$

where W is the load.

The *short bearing solution*, or the *Ocvirk solution*, is shown in Equation A.3, with the load-eccentricity relationship in Equation A.4 [4].

$$p = \frac{\mu\Omega}{C^2}\left(\frac{L^2}{4} - z^2\right) + \frac{3\varepsilon\sin\gamma}{(1+\varepsilon\cos\gamma)^3}, \tag{A.3}$$

where L is the bearing width, and $-\frac{L}{2} \le z \le \frac{L}{2}$.

$$W = \frac{\mu R \Omega L^3}{c^2}\left(\frac{\varepsilon\sqrt{\pi^2(1-\varepsilon^2)+16\varepsilon^2}}{4(1-\varepsilon^2)^2}\right). \tag{A.4}$$

The film rupture location is determined using Equation A.5.

$$\phi = \tan^{-1}\left(\frac{\pi\sqrt{1-\varepsilon^2}}{4\varepsilon}\right). \tag{A.5}$$